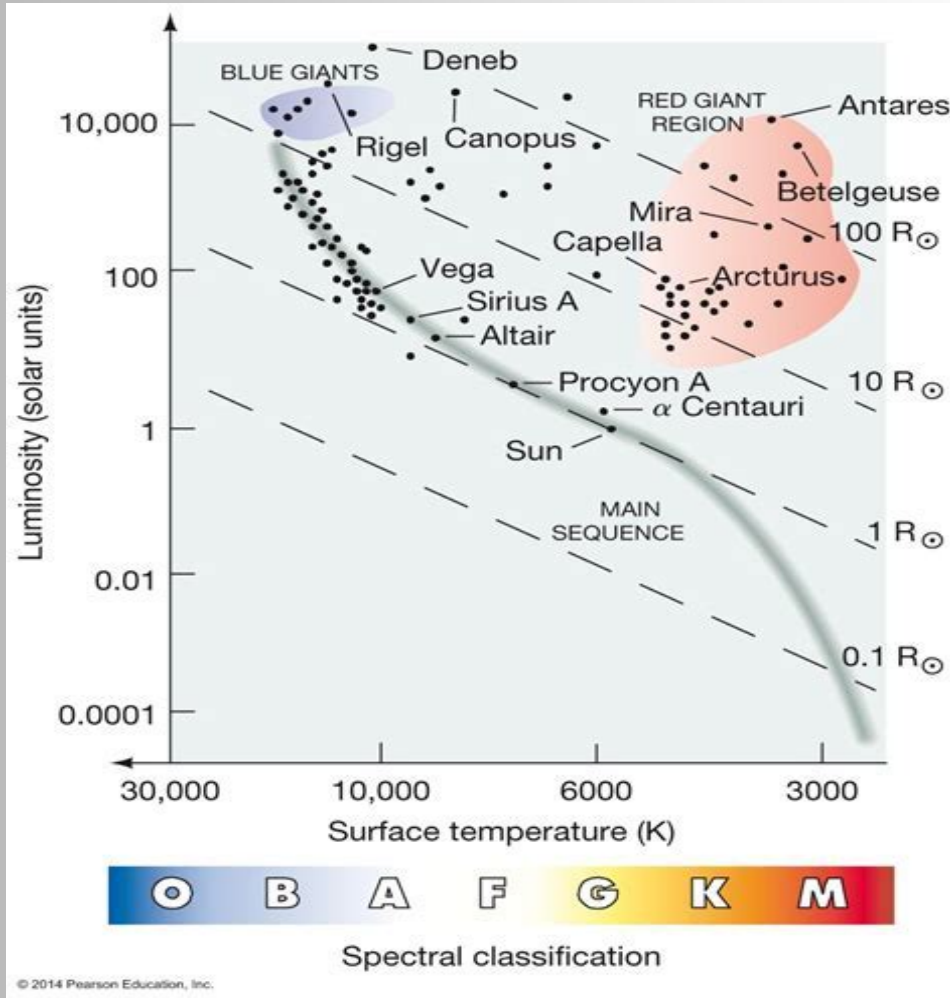


BAV MAGAZINE SPECTROSCOPY

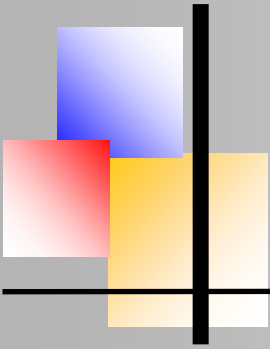


OF THE GERMAN ORGANIZATION & WORKING GROUP VARIABLE STARS BAV

EDITOR
BUNDESDEUTSCHE ARBEITSGEMEINSCHAFT
FÜR VERÄNDERLICHE STERNE E.V. (BAV)
MUNSTERDAMM 90
12169 BERLIN

ISSUE No. 13 06/2023 ISSN 2566-5103





BAV MAGAZINE SPECTROSCOPY



EDITORIAL

From the stars we basically receive only their electromagnetic radiation of different wavelengths, and we “see” essentially only the surface of the radiating bodies. By evaluating the light, we obtain information about:

- the direction of the radiation (positions and movement of the stars)
- the quantity of the radiation (brightness)
- the quality of the radiation (color, spectrum, polarization)

For amateurs, only the narrow band of visible light is easily accessible. In this spectral region, however, both the brightness (photometry) and the spectra of the objects can be examined. Today's amateur astronomy, with its instrumental and computer-assisted equipment, enjoys observation possibilities that were reserved exclusively for professional astronomers until a few years ago.

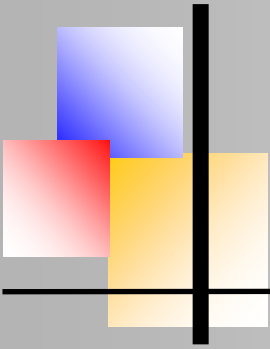
Thanks to the development of CCD technology, the types of observational perspectives have become much more varied. For example, in the area of variable star observation, there are many new possibilities in addition to already existing approaches.

Professional variable star research employs techniques and observation methods to study the physics and atmospheres of the stars in a holistic manner, considering all aspects and occurrences. Thus, this means that the collected radiation must be understood as a complex storage medium of the physical processes on and in the observed star.

This is appropriate for the intensity of the light, as well as for its spectral composition. The linking of brightness measurements and spectroscopy, a matter of course in professional astronomy, reflects this connection.

Along with brightness changes that occur in variable stars (which can occur quite frequently) variable changes in the state of the stars also can take place and often are revealed in the corresponding spectrum.

Ernst Pollmann



BAV MAGAZINE SPECTROSCOPY



Imprint

The BAV MAGAZINE SPECTROSCOPY appears half-yearly from June 2017. Responsibility for publication: German Working Group for Variable Stars e.V. (BAV), Munsterdamm 90, 12169 Berlin

Editorial

Ernst Pollmann, 51375 Leverkusen, Emil-Nolde-Straße 12, ernst-pollmann@t-online.de
Lienhard Pagel, 18311, Klockenhagen Mecklenburger Str. 87, lienhard.pagel@t-online.de
Roland Bücke, 21035 Hamburg, Anna von Gierke Ring 147, rb@buecke.de

The authors are responsible for their contributions.

Coverpicture:

HRDT2 (Astronomy & Astrophysics Royal Observatory of Belgium)

Content

Page

E. Pollmann: Editorial

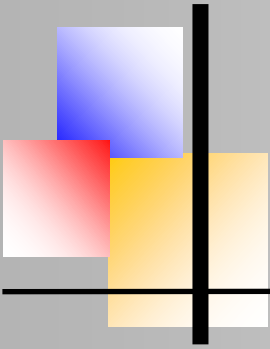
R. Bücke: Atmospheric waterlines in stellar spectra.....1

M. Kolb: Natrium lines in (recurrent) Novae.....7

**E. Pollmann & Philip Bennett: Spectroscopic monitoring
of the 2017-2019 eclipse of VV Cephei.....12**

P. Velez: Automatic spectroscopy observations.....24





Atmospheric waterlines in stellar spectra Roland Bücke, Hamburg (Germany)



Atmospheric lines (also called telluric lines) in the spectra of stars are caused by the absorption of light as it passes through the Earth's atmosphere. In higher resolution spectra of the spectral classes O and B, these lines appear unmistakably, since they only have a few stellar lines. Among other things, the absorptions of the water molecules in the areas of the NaD lines at 5995 Å and the H α line and a strong band of atmospheric oxygen at 6300 Å are striking. The line groups mentioned are in a spectral range that is observed particularly frequently by amateurs.

The spectrum of the Be star ζ Tau shown as an example (Fig. 1) was recorded at a low level above the horizon and with a high water vapor content in the air, so that the water lines are very pronounced despite the relatively low resolution of the spectrum. In this article, I would like to use a few examples to draw attention to the possible influence of these waterlines on the evaluation and interpretation of stellar spectra. Especially in the case of Be stars with very broadened H α emissions, these should not be underestimated and, in my opinion, are not yet adequately taken into account in amateur spectroscopy.

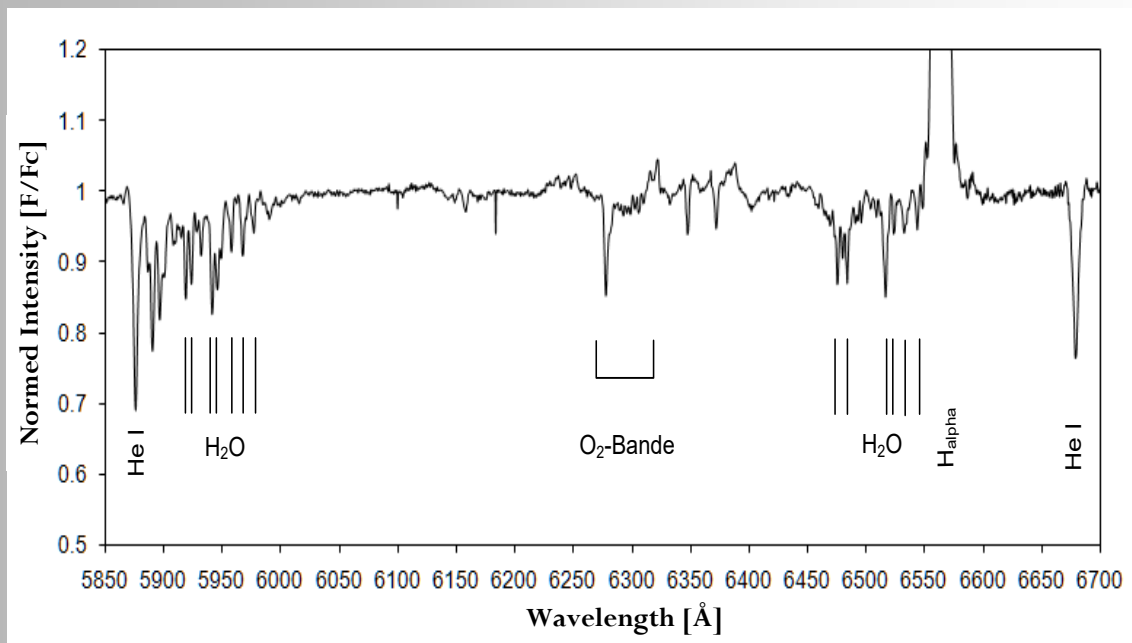
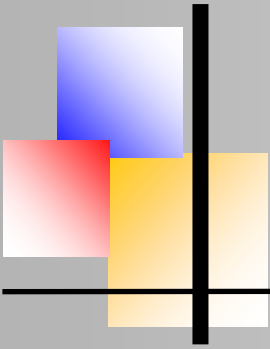


Fig. 1: Spectrum of ζ Tau ($R = 3500$) with strong pronounced atmospheric waterlines



General Appearance

Atmospheric lines are revealed in high-resolution spectra by the fact that, in contrast to the lines of the stellar atmosphere, they are almost unbroadened and are therefore very sharp and strongly absorbing. The physical conditions necessary for widening are absent in the earth's atmosphere. However, as the resolution of the spectrograph decreases, the lines become more and more "washed out" and therefore appear correspondingly wider and less deep. Even if they are hardly or not at all recognizable at low resolution, their influence on the stellar spectrum remains.

The intensity of the telluric lines is determined by the number of absorbing molecules on the light's path through the atmosphere. This depends on a variety of factors, such as the height of the object above the horizon, the height of the observation site above sea level, the humidity, the air pressure, etc. In order to reduce the disturbing influences of the earth's atmosphere on astronomical observations, the modern observatories for professional astronomy are erected on high mountains.

A positive aspect: the calibration with waterlines

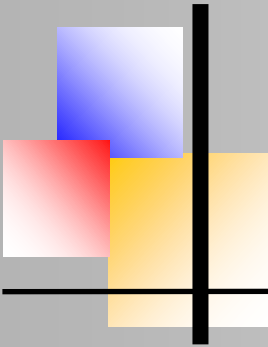
Since telluric lines do not exhibit a Doppler shift (the observer is at rest in relation to the area where the absorptions originate in the earth's atmosphere), they can be used for precise wavelength calibration of spectra. However, only spectra with a sufficiently high resolution from about $R = 8000$ are suitable for this, so that the positions of the lines can be determined with sufficient certainty.

This is usually done by fitting a Gaussian curve. With high-resolution spectra, calibration accuracies are achieved as required for radial velocity measurements. However, calibration with atmospheric waterlines has one major disadvantage: They only cover small spectral ranges, so that precise calibration outside of these is not possible.

Effects on line profiles and line weights (EW values)

Line profiles provide detailed information about the physical conditions in the area of origin of the line in question and the matter that is on the path of the light to us. In particular, the profiles of the emission lines of the hydrogen from Be stars, which change greatly over time, are worthwhile observation objects for the ambitious amateur.

In particular, the line profile of the $H\alpha$ line can be demonstrably falsified by the atmospheric water lines in the line area. Fig. 2 expresses this impressively - without waterline correction, neither the double peak structure nor the change in the V/R ratio are clearly recognizable.



Atmospheric waterlines in stellar spectra

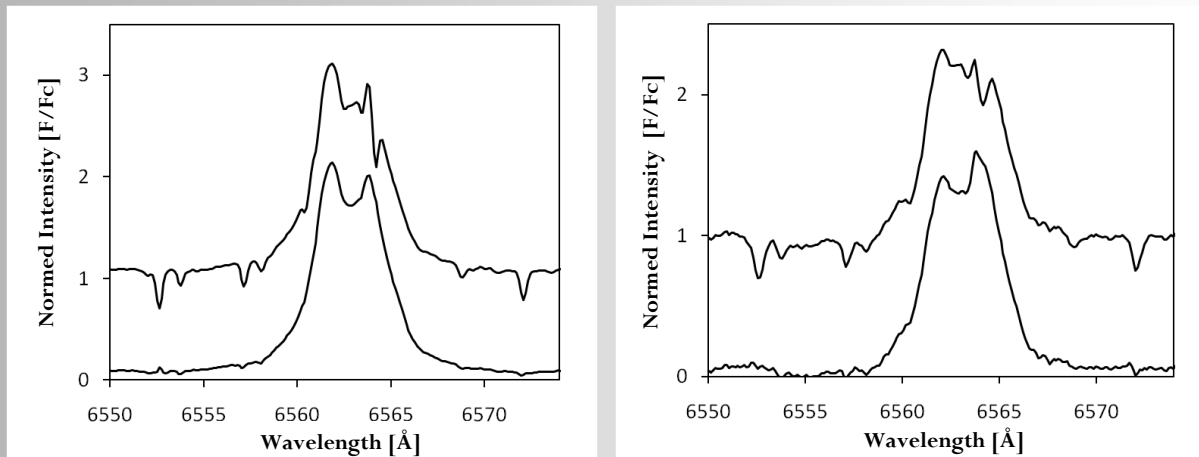


Fig. 2: H α line from delta Sco; top: with waterlines, below: without waterlines; left: spectrum taken by Peter Schlatter, 06/05/2010; right: spectrum taken by Ernst Pollmann, 06/30/2010 b (source: BeSS)

The strength of the line as an integral measured value (EW value) is also affected. Fig. 3 shows a separate measurement series for the development of the EW value of the H α line of γ Cas over time. The telluric absorption lines reduce the EW value of the emission. A closer look also reveals that some temporal changes are largely caused by seasonal influences of the water vapor content of the atmosphere and the height of the object above the horizon. Very faint lines, such as the FeII lines of γ Cas, can sometimes be distorted beyond recognition. Their existence only becomes apparent after the waterline correction (Fig. 4).

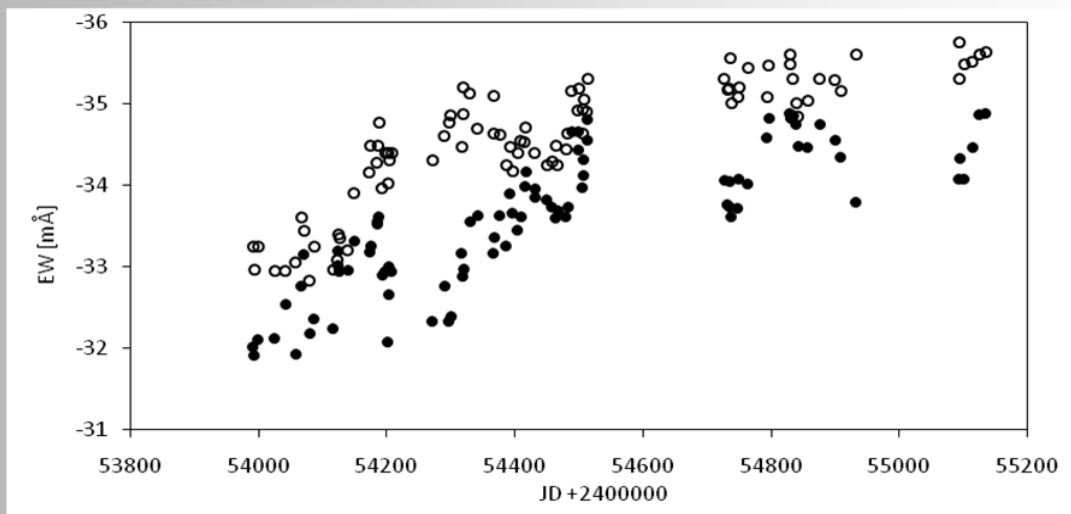


Fig. 3: EW values of γ Cas, black dots: without correction; open circles: with correction

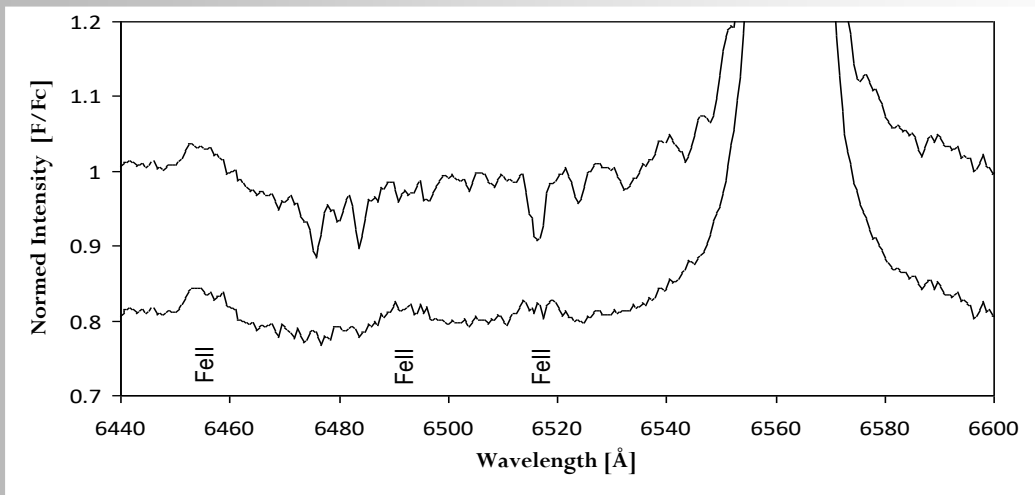
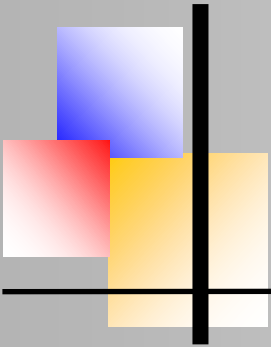


Fig. 4: Spectrum of γ Cas around the $H\alpha$ line

Elimination of water lines and other atmospheric lines

The VSpec program, for example, is very suitable for eliminating atmospheric water lines. Most spectroscopists will certainly use such ready-made solutions without having to worry about the mathematics behind them. Nevertheless, for readers with a deeper interest in this topic, I would like to briefly present my mathematical approach. First, an absorption line spectrum for the lines to be removed in the relevant spectral range must be calculated with the resolution of the spectrum. Then, with such a reference spectrum, the stellar spectrum is cleared of the interfering lines by convolution.

Generating the spectra of telluric lines

The very sharp terrestrial absorption lines are broadened according to the apparatus function of the spectrograph. In a first approximation, the apparatus function can be represented by a Gaussian curve (Eq. 1), the width of which is determined by the resolution of the spectrograph.

$$G_{\lambda} = I_L \cdot e^{-\frac{2.78}{A^2}(\lambda - \lambda_L)^2}$$

I_L = line intensity,

A = resolution of the spectrograph in \AA

λ_L - line wavelength in \AA

Fig. 5 shows the water spectrum in the area of the $H\alpha$ line for different spectral resolutions. This comparison clearly shows that as the spectrograph resolution decreases, fewer and fewer lines can be resolved or only observed as blends.

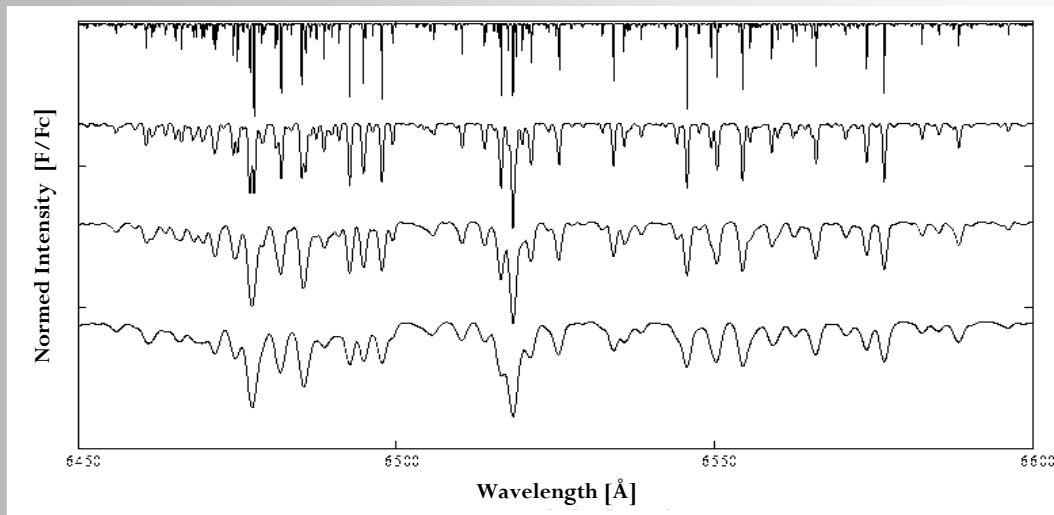
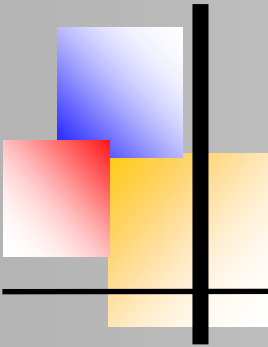


Fig. 5: Absorption spectrum of the terrestrial water lines for different spectral resolutions (from top to bottom: unbroaderened, R=13000, R=6500, R=4300)

Since the vacuum wavelengths for the lines are specified in the HITRAN lists, these must be converted to air. For areas close to the ground, the refractive index for air is approximately 1.00027. Since the index of refraction depends primarily on air pressure, minor corrections must be made according to the altitude of the observation site and the atmospheric conditions at the time of observation.

1. The wavelength of the reference spectrum is to be converted using a suitable interpolation method in such a way that the same interpolation points are obtained for the stellar spectrum.
2. The elimination now takes place with Eq. (2):

$$I(\lambda)_{korr} = \frac{I_{Spektrum}(\lambda)}{k \cdot I_{Referenz}(\lambda) + 1}$$

the factor k is varied until the best result is achieved.

Finally, an example that illustrates how well a correction of telluric lines is possible with the procedure described on this page (Fig. 6).

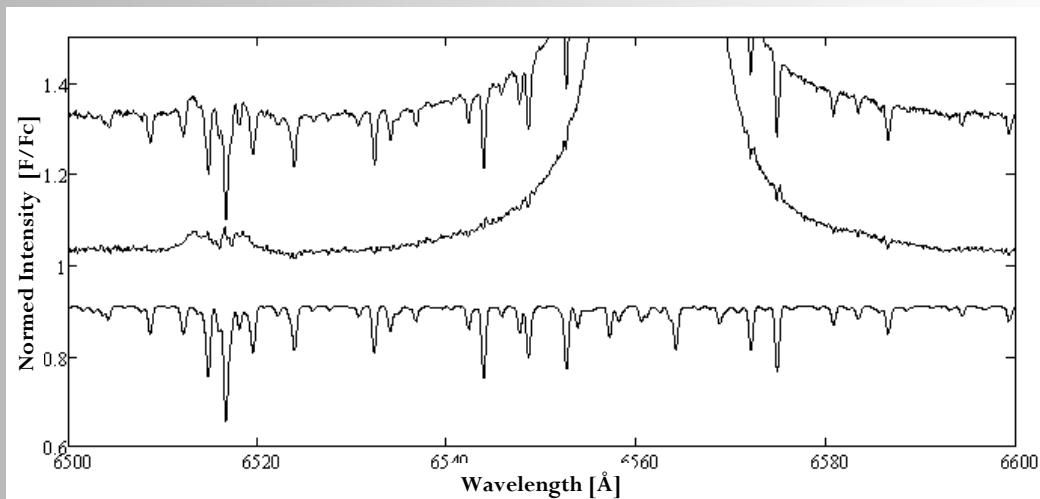


Fig. 6: Spectrum of γ Cas, $R=13000$ (from top to bottom: original spectrum, spectrum without water lines, reference spectrum), Source: BeSS

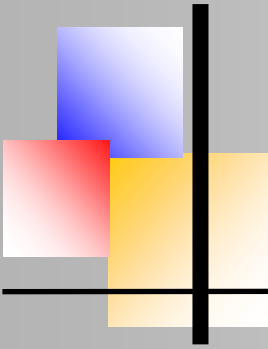
Acknowledgement

This work was prepared using the BeSS database maintained by GEPI, Observatoire de Meudon, France: <http://basebe.obspm.fr>.

I thank the observers Peter Schlatter, Ernst Pollmann and Christian Buil for providing their spectra.

Internet source:

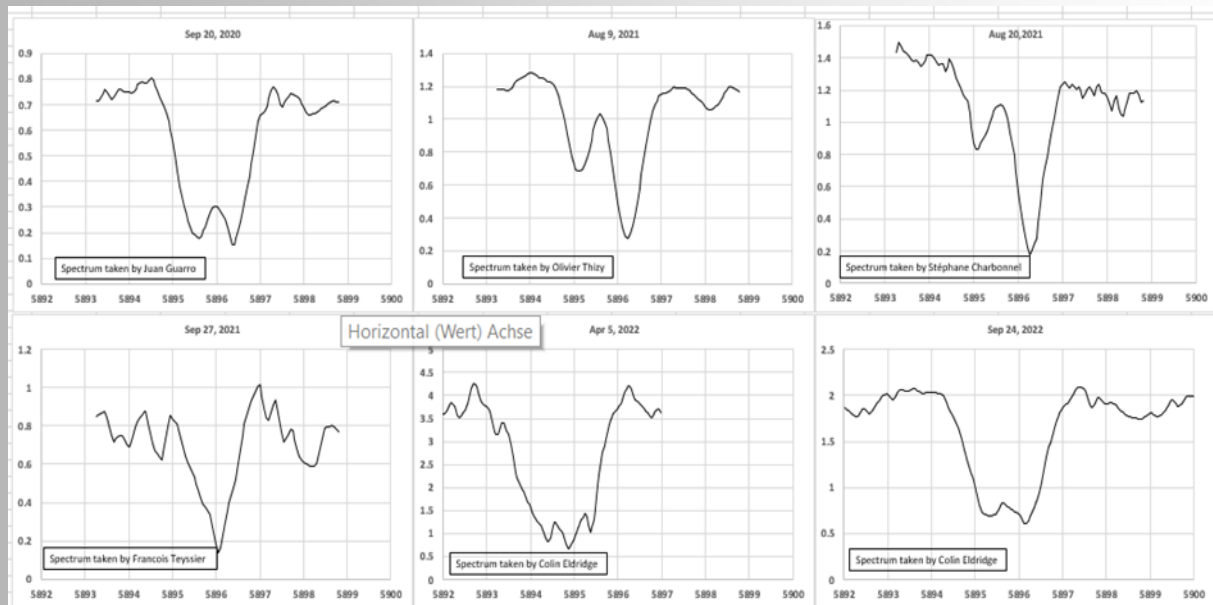
- [1] <http://www.cfa.harvard.edu/HITRAN/>
- [2] http://www.spectralcalc.com/spectral_browser/db_data.php
- [3] <http://basebe.obspm.fr/basebe/>



Natrium lines in (recurrent) Novae Matthias Kolb, Wuppertal, Germany



The development of the Na lines in recurrent Novae RS Oph before, during and after outburst 2021 was subject of a previous article in this journal (https://bav-astro.eu/images/BAVMS_11-2022.pdf). Like for the 2006 outburst, the Na D lines are split into two major features where the more blue-shifted feature was declining substantially during the outburst to appear again after some months. This effect was described by Patat et.al. for the 2006 outburst: The authors identified five features due to the significantly higher resolution. Their interpretation is that two of the five are caused by absorption from interstellar medium, three (on the blue side) associated to absorption from circumstellar material from previous outbursts. This material is heated-up by the nova ejecta shortly after the outburst and the sodium atoms ionize and therefore the absorption features decrease significantly. After some time recombination starts and the lines come back. Fig. 1 shows this effect for the 2021 outburst: In addition to the previous article two

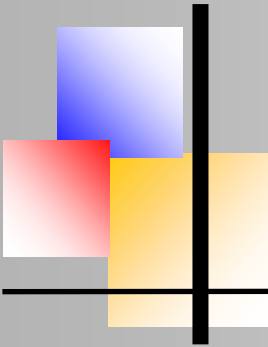


new spectra from 2022 have been added, showing the re-appearance of the dual structure.

Fig 1: Development of Na D1 line before, during, and after 2021 outburst of RS Oph.

Note: Na D2 line left out!

If Patat's explanation holds we could expect similar phenomena for other recurrent novae. Earlier 2022 year we could observe the outburst of U Scorpi. Therefore I looked at spectra



Natrium lines in (recurrent) Novae

resolution from J. Guarro Flo (which are also available in the BAA database), dated June 9 and 10 (two days after maximum V band) with $R=9,000$. The AAVSO database AV Spec has no spectrum with high enough resolution. I could find spectra on the ESO science portal for the 2010 outburst (V_{\max} at January 28) from February 14 until July 5, 2010 and also for April and May 2011). As can be seen from Fig 2 there are two “regular” peaks as can be expected from Na D doublet, no fragmentation visible like in RS Oph.

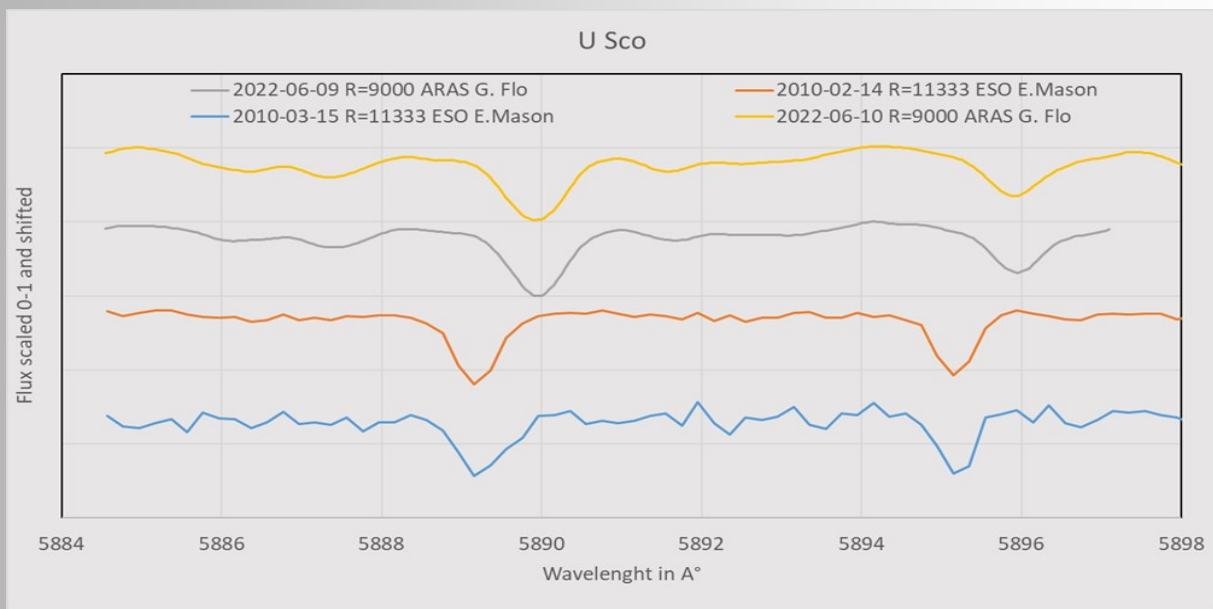
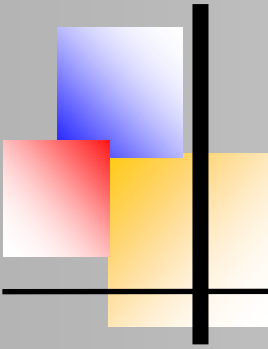


Fig 2: U Sco Na D from spring 2010 and summer 2022, shortly after V max.
Calibration from spectra.

Another example is T Pyx. These recurrent novae showed 2011 last outburst. No spectra available in ARAS, BAA, and AVSpec databases, but several in the ESO science archive. Also here, only a normal NA D doublet is visible after outburst and also a year later.

A possible explanation for the negative detection of similar structures to RS Oph could be that both U Sco as well as T Pyx are recurrent novae, but not symbiotic like RS Oph. Other examples of this special class are T CrB, V475 Sco, and V3890 Sgr. The last outbursts of these novae date back to 1946 2014, and 2019 respectively. I could not find spectra for the latter of the three, but for T CrB and V745 Sco.



Sodium lines in (recurrent) Novae

T CrB: Several spectra from R. Lester with $R=14000$ in the BAA database do show two lines for Na D: the lines show some variation in shape, but no clear structure like RS Oph. For obvious reasons the ESO database has no spectra to offer.

V745 Sco: This one is much more interesting. The ESO archive has quite some spectra from 2014/2015. Laura Chomiuk, now professor at the Michigan State University at East Lansing, MI, is shown as principal investigator for a project with the title *Time Variable Sodium Lines in V745 Sco: Heraldng the Progenitors of Type Ia Supernovae*, which fits exactly to the scope of work of Patat with RS Oph. His publications from 2011 may have triggered this investigation after outburst of V745 Sco three years later. Unfortunately Chomiuk seems not to have published results of the investigation, I could not find it in the ADS database. As a side note: it is worth reading her article from 2021 *New Insights into Classical Novae*.

Fig. 3 shows the relevant region of three spectra from March 23, May 5, 2014 as well as May 1, 2015. The Na lines are very fragmented, covering a range of 5\AA or 250 km/s into the blue.

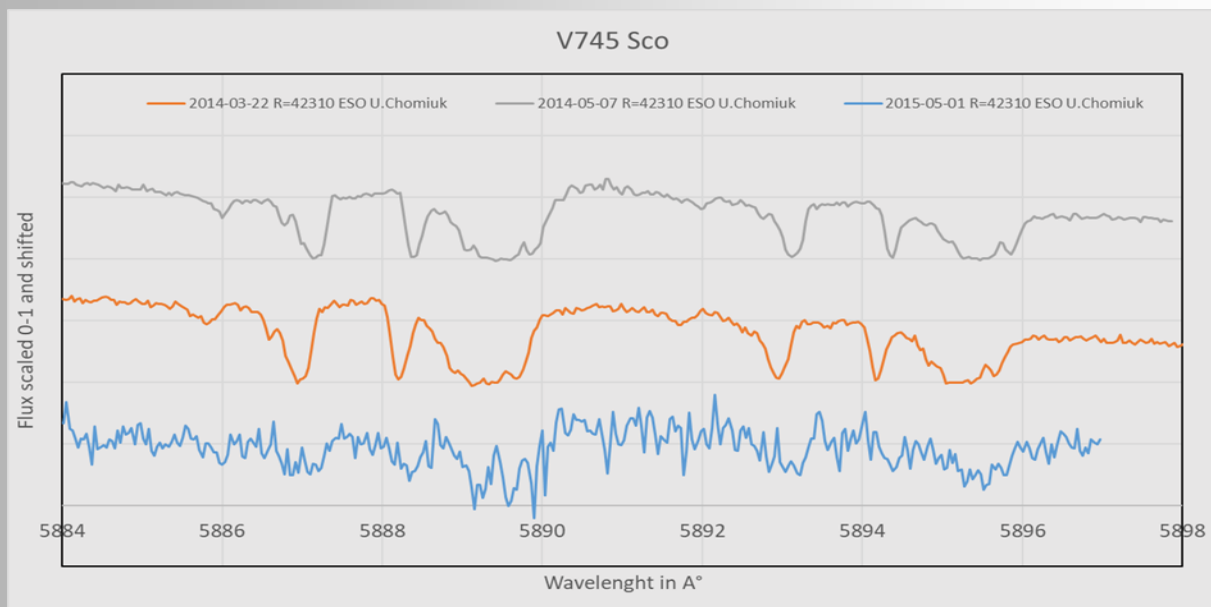
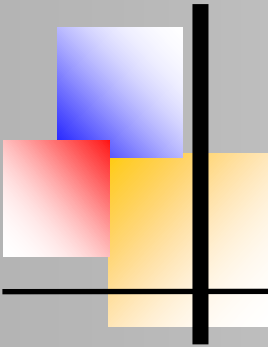


Fig. 3: V745 Sco during and after 2014 outburst

Unfortunately the S/N ratio of the spectrum from May 2015 is very low and changes versus the spectra shortly after the nova outburst in 2014 cannot really be detected. But it seems rather likely that the fragmentation has its origin in the interstellar gas between us and the nova and cannot be compared to the potential circumstellar nova remnant as in RS Oph. This is supported by the following observation.



Natrium lines in (recurrent) Novae

A very fragmented Na doublet in an „ordinary“ nova: V6595 Sgr (N Sgr 2021b)

Looking into ESO spectra for some other novae I found some interesting cases like V6595 Sgr from April 2021. The sodium lines show a very fragmented structure which can already be seen in the ARAS spectrum from J.G.Flo with resolution 9500 (Fig. 4). In comparison two spectra from ESO with $R=34,450$ and $R=107,200$ (!). They all cover the early phase of the Nova (April 9 to 16, 2021). They show the multiple features covering a range of approx. 200 km/s on the blue side of the lab wavelengths. The origin of these blue-shifted features must come from the interstellar gas in that direction of the sky (close to the milky way dust line). A similar pattern is visible in a close-by star from an OB association in 0.1° angular distance from the nova as well as in V5853 Sgr (N Sgr 2016b, not shown in Fig. 4).

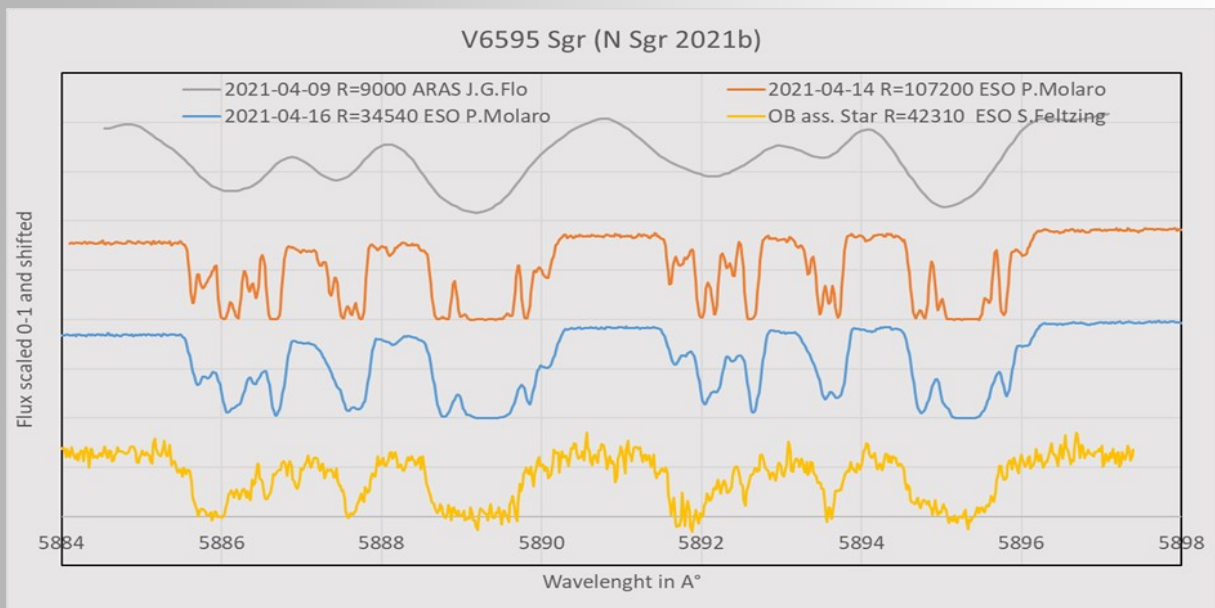
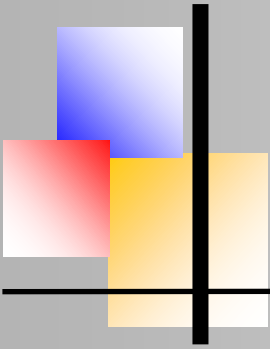


Fig. 4: V6595 Sgr after outburst 2021 and a close-by star from an OB association.

The similarity of the spectra from the recurrent symbiotic nova V745 Sco to the regular nova V6595 Sgr and other stars in this region supports the assumption that the fragmentation is due to interstellar gas and not circumstellar material from previous nova outbursts.

Why is this fragmentation not visible in U Sco? Well, U Sco has an angular distance to V6595 Sgr of 24.6° whereas V745 Sco is only 4.1° away. This is also seen in the dust extinction values A_v calculated with two different methods (NASA/IPAC calculator):



Star	A_v (S+F)	A_v (SFD)
V6595 Sgr	2.36	2.75
bul_sc35-2862	2.57	2.99
V745 Sco	2.22	2.59
U Sco	0.96	1.11

Table 1: Dust extinction parameters calculated with Schlafly & Finkbeiner 2011 and Schlegel et al. 1998 (NASA/IPAC infrared science archive calculator).

Summary

The evolution of the narrow D lines of sodium in the symbiotic recurrent nova RS Oph which Patat et. al. described for the 2006 outburst can be reproduced with spectra taken before, during and after the 2021 outburst. The explanation, that the variability is caused by the ionization (and following recombination) of circumstellar dust from previous outbursts seems plausible. On the other side, similar dynamics cannot be detected in other recurrent novae. Nevertheless, the sodium lines are not always “regular” as expected but may show extreme fragmentation for stars close to the dust line of the milky way like seen in V6595 Sgr or V759 Sco.

Literature:

Patat F., Chugai N. N., Podsiadlowski P., Mason E., Melo C., Pasquini L., A&A, 530, A63 (2011)

Chomiuk L., Metzger B.D., Shen K.J., Ann.Rev. of Astronomy & Astrophysics, Vol. 59 (2021)

Acknowledgements:

Spectra from the following observers were taken out of the ARAS database:

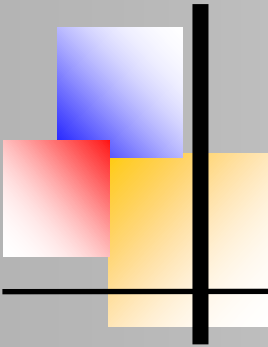
Joan Guarro Flo, Olivier Thizy, Stéphane Charbonnel, and Colin Eldridge <https://ui.adsabs.harvard.edu/abs/2019CoSka..49..217T/abstract>.

http://www.astrosurf.com/aras/Aras_DataBase/DataBase.htm.

ESO library of stellar spectra: <https://www.eso.org/sci/facilities/paranal/decommissioned/isaac/tools/lib.html>

Spectra from principal investigators: P.Molaro, S.Feltzing, U.Chomiuk

NASA/IUPAC Datenbank <https://irsa.ipac.caltech.edu/applications/DUST/>



Spectroscopic Monitoring of the 2017–2019 Eclipse of VV Cephei

Ernst Pollmann (Leverkusen, Germany) & Philip Bennett (Photo)
(Dalhousie University, Halifax, Canada)



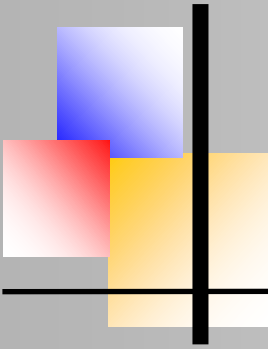
Abstract

VV Cephei is an M supergiant star that eclipses its B-type companion every 20.36 years. It is the eponymous member of the red supergiant + hot main-sequence binaries known as the VV Cephei stars. The red supergiant primary is surrounded by a circumstellar shell due to mass loss via a slow, stellar wind, and this circumstellar material interacts with the hot companion. Spectroscopic observations in the ultraviolet indicate the presence of material accreting onto the hot star from the wind of the M supergiant primary, and the probable presence of an accretion disk around the companion. The hot star and disk produce a local H II “bubble” that results in very prominent H α emission originating from the vicinity of the companion. In this work, we report on a continuing campaign of spectroscopic observations of H α emission from VV Cep over the period 2015–2020 by amateur observers of the ARAS spectroscopy group. We also present a newly discovered 42-day period variability in the equivalent width of this H α emission.

Introduction

VV Cephei (M2 Iab + B0-2 V) is the best known, brightest, and eponymous member of the composite spectrum binaries with M supergiant primary stars and hot B-type main-sequence companions. The M supergiant primary is one of the largest known stars in size, with a radius of about 1000 solar radii. Both the M supergiant and its companion are comparably massive, with masses near 20 solar masses. The VV Cep binary system is observed nearly edge-on, and undergoes total eclipses every 20.36 years, which is one of the longest known periods of any eclipsing binary. This binary has been a system of particular interest for almost a century, following McLaughlin’s (1936) discovery that the binary was eclipsing. It is one of the most massive, longest-period eclipsing binary systems known. McLaughlin (1934) first reported on the composite-spectrum binary, with its broad hydrogen emission lines and H and K lines of ionized calcium (Ca II). Subsequently, McLaughlin (1936) announced that the hot star in VV Cep had been eclipsed, establishing the system as an eclipsing binary. Goedicke (1939) carried out the first detailed spectroscopic analyses of this system. Wright (1970) presented an orbital solution for the M supergiant primary. Hutchings and Wright (1971) and Wright (1977) recognized that the H α emission came from around the hot companion and used this prominent emission line to derive orbits of the secondary star.

The visible spectrum longward of 5000 Å, except for the very prominent emission line of H α , is that of the luminous red supergiant primary. However, shortward of 4000 Å, the spectrum of the hot companion becomes increasingly dominant.



Spectroscopic Monitoring of the 2017–2019 Eclipse of VV Cephei

In VV Cephei itself, the evolved M supergiant is surrounded by an extensive shell of circumstellar material due to mass lost from the red supergiant via a stellar wind, and this wind completely envelops the companion's orbit. Some of this material is captured by the hot companion, resulting in an accretion region around the B-type star, and emission from this accretion region mostly obscures the photospheric spectrum of the hot star in the ultraviolet. The companion is hot enough, at around spectral type B1V, to ionize a local "bubble" of circumstellar gas, and it is recombination of ionized hydrogen in this H II region that produces the prominent H α emission, as well as strong emission in the other hydrogen Balmer lines and in the Balmer continuum in the ultraviolet (see Fig. 1). The ultraviolet spectrum is characterized by numerous emission lines of Fe II, which are probably pumped by strong emission in the Lyman- β line (Bauer and Bennett 2000) from the same H II region.

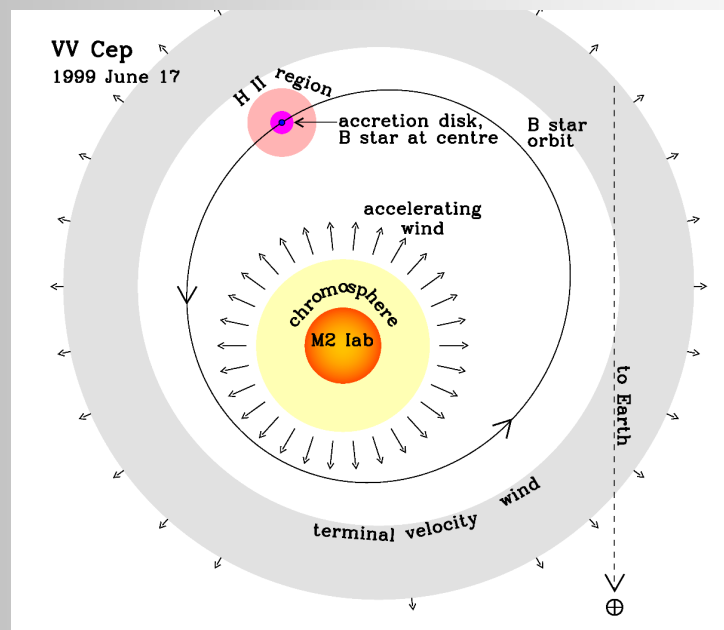
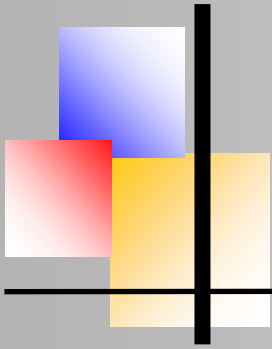


Fig. 1: The orbit and structure in the orbital plane of the VV Cephei binary on 1999 June 17, drawn to scale (adapted from Bennett and Bauer 2015).

As noted, out of eclipse, the H α spectral line at 6563 Å is particularly prominent in this star, with a peak emission flux several times that of the M star's continuum. The H α line is one of the few features in the visible spectrum that arises from the hot companion, as established by a radial velocity behavior that runs counter to that of the red supergiant. Observations of the H α emission line provide valuable information on the difficult-to-observe companion, and of a possible accretion disk around the hot companion (Wright 1977; Kawabata *et al.* 1981;



Spectroscopic Monitoring of the 2017–2019 Eclipse of VV Cephei

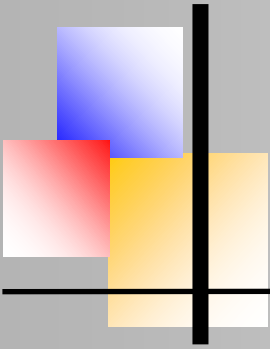
Moellenhoff and Schaifers 1978, 1981). Despite the prominent wind accretion and interaction in this binary, direct mass transfer via Roche lobe overflow does not appear to be taking place. The spectroscopic orbit of the M supergiant is fairly well established, and the orbit is decidedly eccentric, with an eccentricity of $e = 0.35$ (Wright 1970). The two stars are reasonably well-separated, with a ratio of orbit semi-major axis to M star radius (a / R_1) of about 5, and a periastron separation to M star radius of ~ 3.3 (Bennett and Bauer 2015). Since mass transfer binaries undergoing Roche lobe overflow invariably have orbits circularized by tidal interactions, the eccentric nature of the VV Cep orbit suggests that VV Cep has never undergone significant episodes of Roche lobe mass transfer.

The ultraviolet spectrum appears to be largely of nonstellar origin, with strong inverse P Cygni line profiles of ionized metal lines (especially Fe II), and a continuum that varies by up to a factor of 3 outside of eclipse. Both the inverse P Cygni profiles—indicative of infalling circumstellar gas—and the variable Balmer emission continuum suggest an accretion source for the nonstellar UV spectrum (Bauer and Bennett 2000; Bennett and Bauer 2015). The spectroscopic orbit (Wright 1977) implies both stars are comparably massive, so the companion must be a luminous main-sequence star, but even so, the stellar source contributes only 30–50 % of the UV luminosity. The rest of the luminosity must come from the accretion region, which is probably organized as an accretion disk around the hot star. The nonstellar component of the spectrum in the UV consists of Balmer continuum emission, and metal line emission (especially Fe II) powered by fluorescence with Lyman emission lines. The accretion disk is also hot, and appears to contribute to much of the ionization of neutral circumstellar hydrogen in a local, confined bubble around the hot star (Fig. 1).

In this paper, we present an extensive set of high-cadence spectroscopic monitoring of the $H\alpha$ emission line in VV Cep over the entire eclipse period of nearly three years. This continues the work previously presented by Pollmann, Bennett, and Hopkins (2016) and Pollmann *et al.* (2018). We also report on a newly discovered 42-day oscillation in the equivalent width (EW) and peak fluxes, and a 51-day radial velocity oscillation in the blue (V) component of the double-peaked $H\alpha$ emission line. We attribute these periodic variations to the precession of the accretion disk around the hot B-type companion.

Observations and analysis

Long-term monitoring of the $H\alpha$ region of the spectrum of VV Cep started in July 1996 (by EP) to observe the 1997–1999 eclipse, and has continued for 24 years to the present day. Since April 2010, observers of the *Astronomical Ring for Access to Spectroscopy (ARAS)* spectroscopy group have been involved in, and contributed substantially to, this long-term monitoring campaign. In 2015, a combined photometric and spectroscopic campaign was organized by J. Hopkins,



Spectroscopic Monitoring of the 2017–2019 Eclipse of VV Cephei

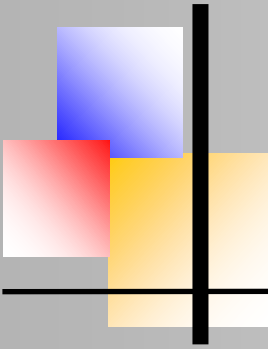
P. Bennett, and E. Pollmann to monitor the recent 2017–2019 eclipse. This eclipse began (first contact) in continuum light, around the beginning of September 2017, and ended (fourth contact) at the start of April 2019. Over this period, medium-resolution spectroscopic observations were obtained in the red spectral region centered on $H\alpha$, using commercially available instrumentation such as the Shelyak Instruments LHires III spectrograph ($R \sim 17000$) and a CCD detector. We present a summary of the results of this observing program in this paper. In Fig. 2, we show a typical LHires III spectrum of VV Cep observed in the red spectral region out of eclipse, with its central self-absorption feature dividing the observed $H\alpha$ emission profile into characteristic blue and red components.

For each spectrum, the total $H\alpha$ equivalent width (EW), the EW and peak flux of the blue (V) and red (R) components, and radial velocity of the blue (V) emission component were measured. The total $H\alpha$ EW variation over the entire 24-year observational period (see Fig. 3) shows considerable variation outside of eclipse on both long and short timescales. Remarkably, weak, narrow $H\alpha$ emission remains present even at mid-eclipse, as can be seen from Fig. 4. This emission must be coming from spatially extended (and low velocity) regions far enough from the hot star so as to remain visible at mid-eclipse.

The slow $H\alpha$ EW variation, occurring on decadal timescales (Fig. 3, dashed curve), correlates with the orbital separation of the two stars, with the largest emission flux occurring near periastron. We report here on the discovery of a rapid 42-day variability that is also present in the EWs and peak fluxes of both the V and R components. A similar 51-day variability is present in the radial velocity of the V component. Surprisingly, this 42-day variability persists through total eclipse, as can be seen from Figure 5.

The continuous and high-cadence nature of these $H\alpha$ observations allows the time-variation of the $H\alpha$ red (R) and the blue (V) emission components to be analyzed in unprecedented detail. In principle, a detailed analysis of the $H\alpha$ profile over the course of the eclipse should permit the geometry of the $H\alpha$ emitting region to be determined.

For this work, we simply present the results and an analysis of the period of the EW and the peak fluxes of the $H\alpha$ V and R emission components and the radial velocity (RV) variation of the V emission component, and defer that complete analysis to a future work. Fig. 6 shows the behavior of the EW and peak fluxes for the V and R components over the course of the eclipse. In particular, the asymmetric nature of the V / R eclipse curve, with its minimum occurring well prior to mid-eclipse, implies that the eclipse of the V component of the $H\alpha$ emission during ingress proceeds much more quickly than that of the R component.



Spectroscopic Monitoring of the 2017–2019 Eclipse of VV Cephei

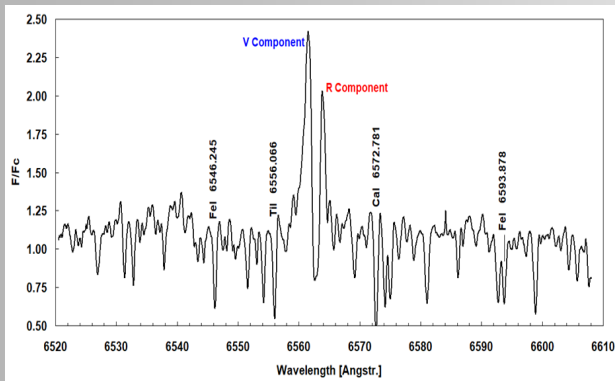


Fig. 2: Typical out-of-eclipse spectrum of VV Cep showing double-peaked H α emission

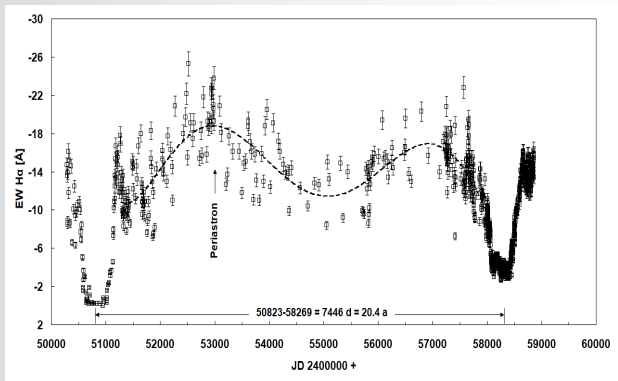


Fig. 3: H α equivalent width (EW) from 1996 to 2020

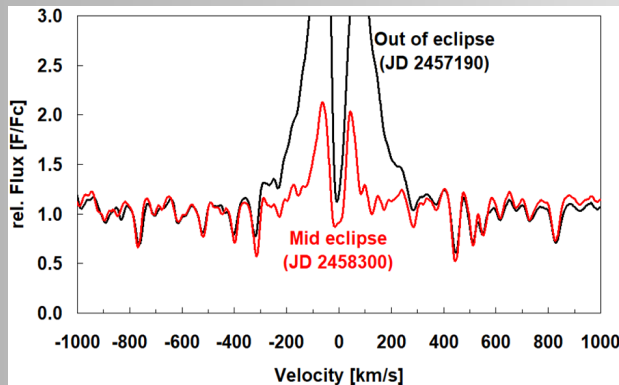


Fig. 4: The narrow H α profile during totality implies the emission here comes from a low velocity region extending beyond the occulting M supergiant, compared to the much broader out-of-eclipse profiles from the accretion disk. Only about 25% of the total flux comes from this extended region.

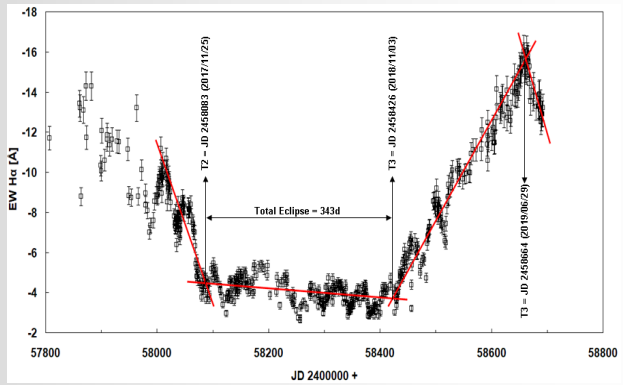
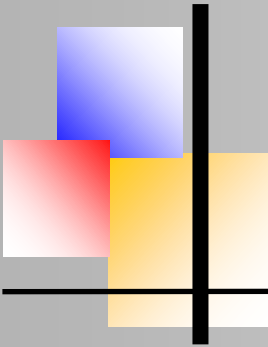


Fig. 5: H α emission EW for the 2017–2019 eclipse. The 42-day variability persists

The AVE code of Barbera (1998) was used to carry out the PDM analysis. Results of this period analysis of the H α emission line EW and of the peak flux of both V and R components of nearly 1000 spectra indicate a significant period of about 42 days. This 42-day period variation is shown in Fig. 7 for the EW of the V and R components (left panels), as well as for the peak flux (right panels) of both emission components. The 42-day variability is confirmed by a periodogram of the V / R ratio, shown in Fig. 8. The source of the observed H α variability



BAV MAGAZINE SPECTROSCOPY



Spectroscopic Monitoring of the 2017–2019 Eclipse of VV Cephei

is probably precession of the accretion disk. Although presumably oriented perpendicular to the hot star's rotation axis, this accretion disk need not lie exactly in the orbital plane of the binary. In this situation, the M supergiant would exert a torque on the accretion disk, accounting for the observed precession.

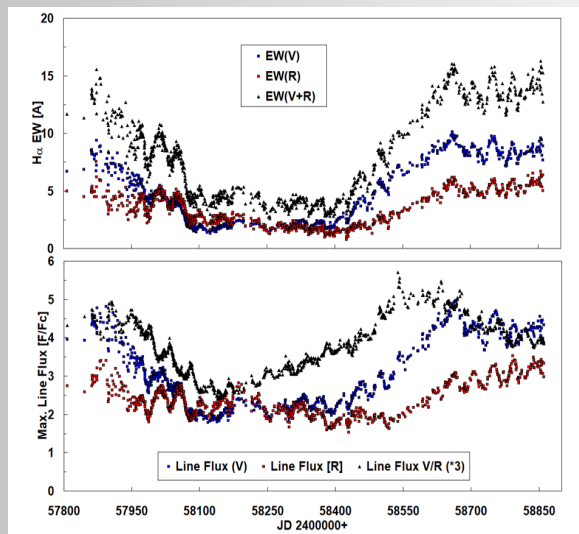


Fig. 6: Periodic variability of EW (left) and peak line flux (right). Both periods are ~ 42 days

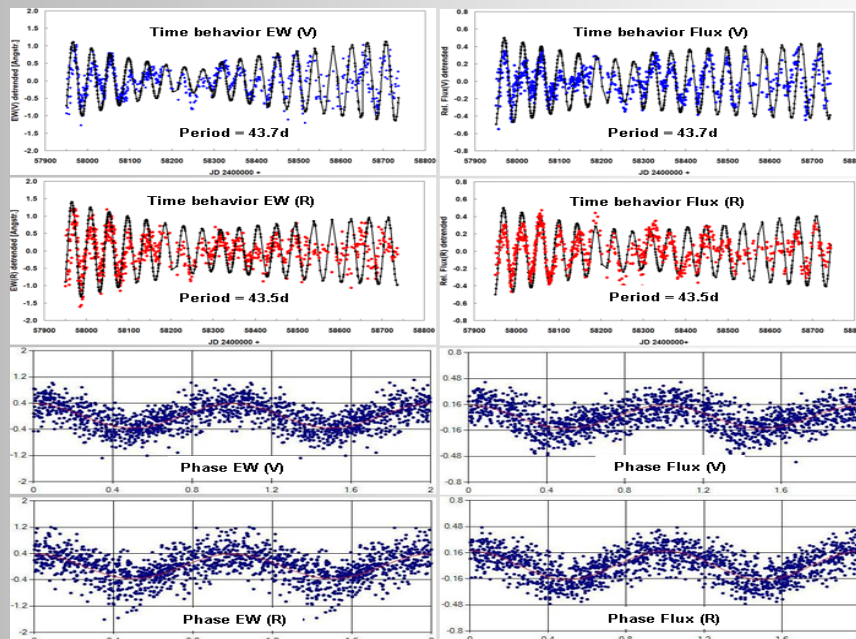
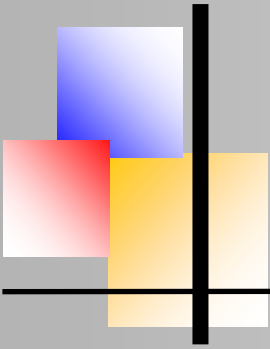


Fig. 7: Periodic variability of EW (left) and peak line flux (right). Both periods are ~ 42 days



Spectroscopic Monitoring of the 2017–2019 Eclipse of VV Cephei

This variability resembles the 58-day semi-regular variability reported by Baldinelli *et al.* (1979), who obtained non-standard R-band photometry (using 103aE plates + RG1 filter) of VV Cep from 1976 to 1978. However, the H α variability described here would seem to be an order of magnitude too small in amplitude to produce the ~ 0.1 -magnitude variation in R flux seen by Baldinelli *et al.* (1979).

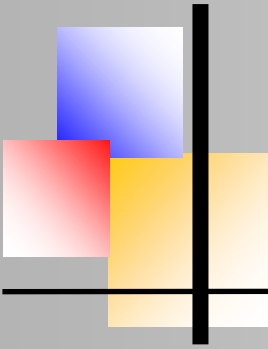
A precessing accretion disk rotation axis with a period of 42 days should result in a similar radial velocity variability. Analysis of more than 400 medium-resolution spectra of VV Cep obtained from 2018 January to 2020 January confirms a similar short periodic variability in the radial velocity of the H α V component. However, a period analysis (see Fig. 9) of the velocity residuals (after subtraction of a smooth trend) gives a period of 51 days instead, but with relatively little power in this period, which only accounts for about one-third of the amplitude of the total short period variability.

Note that the radial velocity measurements were carried out with respect to the M supergiant reference frame. Variation in the width of the central absorption near eclipse might also alias the derived V component radial velocities. In any case, the radial velocity time series analysed here is relatively short. We will revisit the radial velocity analysis after more data have been obtained, and after carrying out a proper subtraction of the orbital solution first.

A proposed model

As summarized in the introduction, recombination of ionized hydrogen (H⁺) in an H II region around the hot star and the accretion disk in VV Cep produces the observed H α emission peak. The H α emission profile is broadened by the high velocities present in the infalling gas, as well as from gas in the accretion disk rapidly orbiting the hot star. The low velocity wind enveloping the entire binary star system results in absorption at velocities near the center of the H α line profile, resulting in a characteristic double-peaked emission profile with separate blue (V) and red (R) emission components.

The spectroscopic orbit implies the hot companion is also a massive star, and that must be (from its mass, and position on the main sequence) an early B star, probably of spectral class B0–2 V. It is difficult to be more precise because the UV spectrum is non-stellar. Moreover, the hot companion is not a compact object in the usual sense. Therefore, it is unlikely that gravitational accretion is the source of the energy powering the non-stellar UV source. The nature of the nonstellar luminosity (hydrogen Balmer and Lyman line emission, and Balmer continuum emission) is that of a recombination spectrum. This suggests the non-stellar emission is being powered by the local ionization of circumstellar hydrogen by the extreme ultraviolet (EUV)



Spectroscopic Monitoring of the 2017–2019 Eclipse of VV Cephei

radiation field (i.e., at wavelengths shortward of 912 \AA) of the hot companion star, with some contribution from the hot gas accreting around the companion star. In this scenario, the EUV continuum of the hot star and accretion region is being reprocessed into hydrogen recombination emission. This process, which depends on the local circumstellar hydrogen density and accretion disk orientation, is what we propose to cause the variable nature of the UV spectrum of VV Cep.

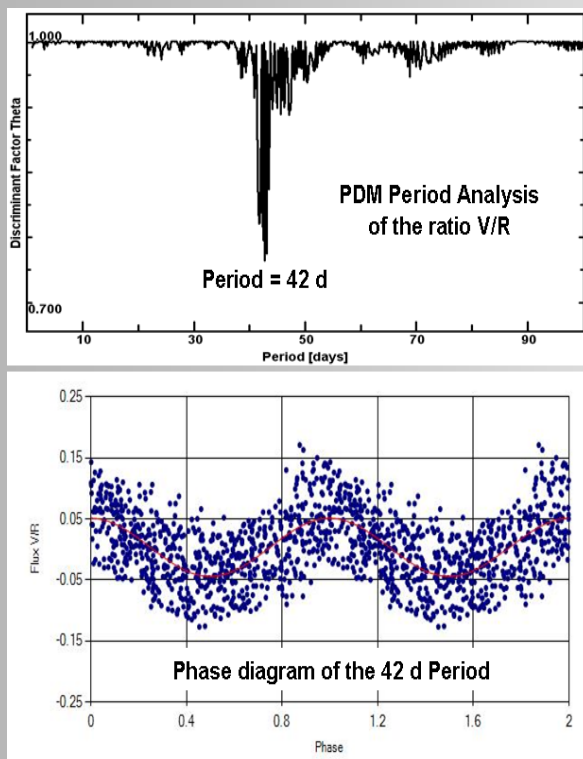


Fig. 8: V / R period analysis. Top: PDM periodogram. Bottom: V / R values phased to 42-day period.

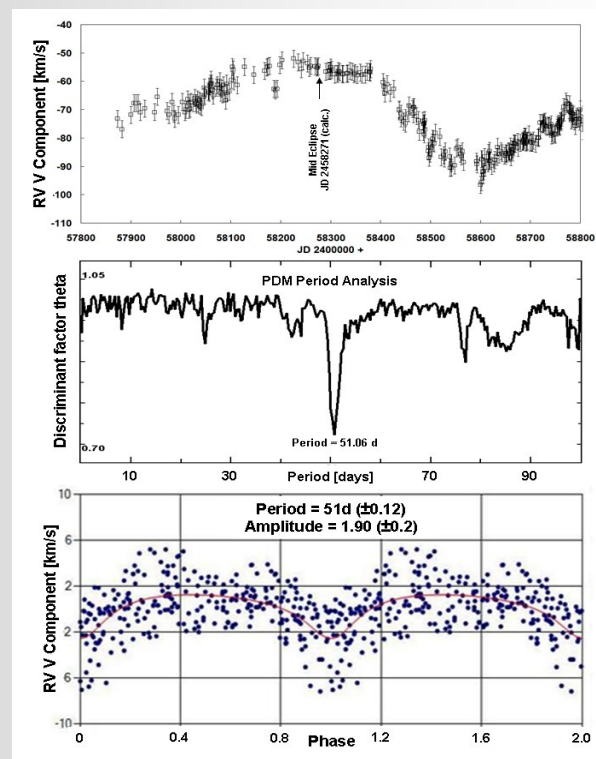
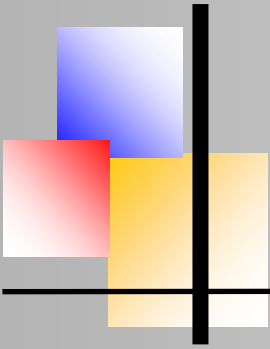


Fig. 9: Radial velocity analysis of the V component of the $H\alpha$ emission. Top: radial velocity of the $H\alpha$ V component. Middle: Period analysis of the detrended data. Bottom: Phase plot of the radial velocity time series for the derived 51-day period.

The size of the B star and its accretion disk, which together produce the UV continuum, are small compared to the M supergiant. We know this because the UV light curve drops quickly to zero during total eclipse, implying that the UV continuum flux comes from a small emitting volume, consistent with a hot star surrounded by a compact accretion disk source. But about 20–25% of the $H\alpha$ flux remains present even at mid-eclipse, so that some of this emission must come from an extended region on the sky that is larger than the projected disk of the M star.



Spectroscopic Monitoring of the 2017–2019 Eclipse of VV Cephei

A more detailed analysis of the evolution of the $H\alpha$ profile during the eclipse now underway should provide valuable constraints on the size and structure of the emitting volume.

The observed 42-day period of $H\alpha$ variability is typical of Be star disk precession periods (Schaefer *et al.* 2010) and it is tempting to suspect that mechanism (precession of the accretion disk) also causes the $H\alpha$ variability in VV Cep, with its accretion disk. But the situation is more complicated than this because the accretion region in VV Cep is totally eclipsed for 19 months during totality. This behavior imposes a severe constraint on the process responsible for the variability. The rapidity of the 42-day variability implies this occurs on small physical scales. This is because a region undergoing a coherent variation cannot be larger than the distance over which the physical disturbance responsible for the variability propagates during the period of the variation. But for the variability to remain present during total eclipse, when the hot star and its accretion disk are totally eclipsed, requires that the precessing disk be communicating that information to a region outside the eclipsed volume. Since typical wind velocities in VV Cep, away from the immediate vicinity of the hot star, are $\sim 20 \text{ km s}^{-1}$, wind travel times to cross an M star diameter (~ 1000 solar radii) are about a year, or much longer than 42 days. The orbital velocities of both stars are of comparable speeds: $\sim 20 \text{ km s}^{-1}$. There is no evidence of higher velocity flows on large scales in VV Cep. Therefore, the source of the variation cannot be gas flows or winds originating with the accretion disk—the velocities are just too slow.

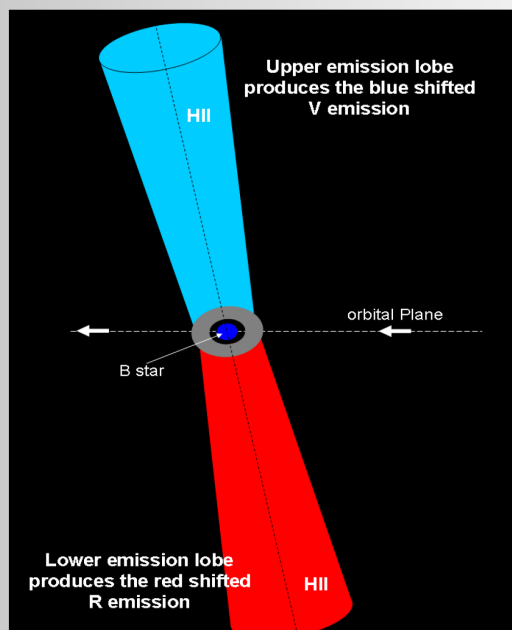
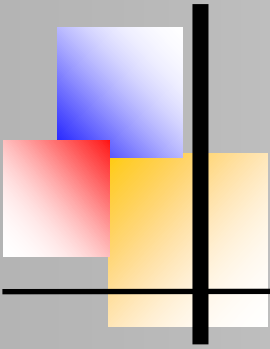


Fig. 10: Model of two $H\alpha$ emission lobes extending above and below the orbital plane from the precessing accretion disk.



Spectroscopic Monitoring of the 2017–2019 Eclipse of VV Cephei

This leaves radiation as the only obvious mechanism fast enough to propagate the 42-day variability over a region larger than that of the M supergiant's radius. The light travel time to cross the M supergiant radius (~ 1000 solar radii) is less than an hour. The propagating radiation cannot be $H\alpha$ directly because $n = 2$ level populations of H I are insufficient to scatter $H\alpha$ light in the relatively cool circumstellar gas around VV Cep. Instead, we propose that extreme UV (EUV) radiation emitted by the accretion disk and hot star ionizes neutral hydrogen gas in two lobes directed above and below the plane of the accretion disk (Fig. 10).

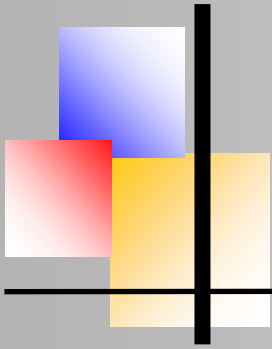
Observations of VV Cep in the ultraviolet with the Hubble Space Telescope (Bauer, Gull, and Bennett 2008) demonstrated the existence of spatially extended emission in strong lines of Fe II. These prominent ultraviolet emission lines are excited by Lyman- β emission from the same recombination process into the hydrogen $n = 3$ level that produces the observed $H\alpha$ emission.

In this model, it is the geometry of the H II region emission lobes, varying with the precession of the accretion disk, that gives rise to the 42-day $H\alpha$ variability. As the disk precesses, these cones of ionization sweep through the neutral circumstellar wind in VV Cep much like a searchlight beam. Inside each H II lobe, circumstellar neutral hydrogen is ionized to H^+ by the disk's EUV radiation, and then recombines to produce $H\alpha$ and higher Balmer line emission.

The precession of the disk results in a modulation of the strength, and radial velocity, of the resulting $H\alpha$ emission, which depends on the geometry of the bipolar emission cones relative to the stellar wind and the position of the eclipsing supergiant. Out of eclipse, $H\alpha$ emission from the H II region near the precessing accretion source is also observed directly. This model accounts for the continued presence of the 42-day $H\alpha$ emission flux variability during total eclipse.

The $H\alpha$ emission lobes are not exactly perpendicular to, but are obliquely inclined, to our line of sight due to the $i \approx 80^\circ$ inclination of the orbital plane of VV Cep. The blue-shifted (V) emission comes from the lobe which opens towards the observer, while the red-shifted (R) emission comes from the lobe opening away from the observer. In addition, the blue V lobe must be more occulted by the red supergiant than the R lobe at the start of the eclipse, because the V lobe fluxes decline more steeply at eclipse ingress.

We require this geometry to explain the asymmetric nature of the V and R curves. Further, the significantly narrower profile shape of the $H\alpha$ emission during total eclipse (seen as red curve in Figure 4) implies a lower velocity source far from the accretion disc, confirming that not all the $H\alpha$ emission comes from the immediate vicinity of the accretion disc.



Conclusions

We present medium-resolution ($R \sim 17000$), high cadence observations of the $H\alpha$ emission line in VV Cep, observed by members of the *ARAS* group from 2010 to the present, and report the discovery of a rapid 42-day variability that is present in the EWs and peak fluxes of both the V and R components. A similar 51-day variability is present in the radial velocity of the V component. Surprisingly, this variability persists through total eclipse, when the hot companion star and surrounding accretion region are totally eclipsed.

To explain the continuation of the 42-day variability through total eclipse, we propose a model in which lobes of neutral hydrogen gas are ionized by extreme ultraviolet radiation from a precessing accretion disk around the hot companion star in this massive binary system. Recombination from the resulting H II region produces the observed Balmer continuum and line emission, including the prominent $H\alpha$ emission.

As the accretion disk precesses with its 42-day period, the H II ionization lobes directed away from the disk sweep through the circumstellar gas around the M supergiant, producing the observed periodic variability in $H\alpha$ fluxes and radial velocity, even when the accretion region itself is eclipsed.

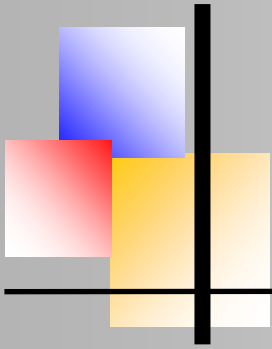
Acknowledgements

We thank all observers of this campaign, without whose great cooperation such an extensive investigation would not have been possible:

E. Bertrand, J. J. Boussat, E. Bryssinck, Ch. Buil, Ch. Revol, St. Charbonnel, Dong Li, P. Fosaneli, J. Foster, O. Garde, Th. Griga, J. Guarro, H. Kalbermatten, M. Keiser, K. Prast, F. Neußer, J. N. Terry, Ch. Kreider, B. Koch, Th. Lemoult, J. Martin, C. Sawicki, O. Thizy, F. Teyssier, T. Lester, J. Schirmer, M. Schwarz, P. Somogyi, Th. Garrel, M. Trypsteen, St. Ubaud, V. Desnoux, U. Zurmühl, A. Stiewing, S. Hold, and D. Hyde.

References

- Barbera, R. 1998, ave code, version 2.51 (<http://www.gea.cesca.es>).
- Bardinelli, L., Ghedini, S., and Marmi, S. 1979, *Inf. Bull. Var. Stars*, No. 1675, 1.
- Bauer, W. H., and Bennett, P. D. 2000, *Publ. Astron. Soc. Pacific*, **112**, 31.
- Bauer, W. H., Gull, T. R., and Bennett, P. D. 2008, *Astron. J.*, **136**, 1312.
- Bennett, P. D., and Bauer, W. H. 2015, in *Giants of Eclipse: The ζ Aur Stars and Other Binary Systems*, eds. T. Ake, E. Griffin, *Astrophys. Space Sci. Libr.* 408, Springer International Publishing, Cham, Switzerland, 85.



BAV MAGAZINE SPECTROSCOPY

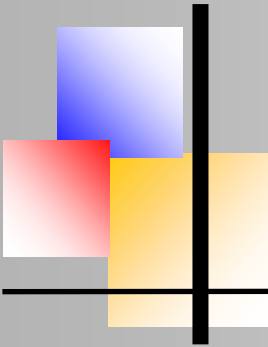


Spectroscopic Monitoring of the 2017–2019 Eclipse of VV Cephei

References

- Cowley, A. P. 1969, *Publ. Astron. Soc. Pacific*, **81**, 297.
- Goedicke, V. 1939, *Publ. Obs. Univ. Michigan*, **8**, 1.
- Hutchings, J. B., and Wright, K. O. 1971, *Mon. Not. Roy. Astron. Soc.*, **155**, 203.
- Kawabata, S., Saijo, K., Sato, H., and Saito, M. 1981, *Publ. Astron. Soc. Japan*, **33**, 177.
- McLaughlin, D. B. 1934, *Astrophys. J.*, **79**, 380.
- McLaughlin, D. B. 1936, *Harvard Coll. Obs. Announcement Card*, No. 397.
- Moellenhoff, C., and Schaifers, K. 1978, *Astron. Astrophys.*, **64**, 253.
- Moellenhoff, C., and Schaifers, K. 1981, *Astron. Astrophys.*, **94**, 333.
- Pollmann, E., Bennett, P. D., and Hopkins, J. L. 2016, *Inf. Bull. Var. Stars*, No. 6156, 1.
- Pollmann, E., Bennett, P. D., Vollmann, W., and Somogyi, P. 2018, *Inf. Bull. Var. Stars*, No. 6249, 1.
- Schaefer, G., *et al.* 2010, *Astron. J.*, **140**, 1838.
- Wright, K. O. 1970, *Vistas Astron.*, **12**, 147.
- Wright, K. O. 1977, *J. Roy. Astron. Soc. Canada*, **71**, 152.





Automating spectroscope observations

Peter Velez, Canberra, Australia, peter@oblaw.net.au



This article describes how I was able to automate spectroscope observations using off-the-shelf software products. The approach I have chosen is basically an individual solution that would possibly be operated in a modified form by other practical amateurs.

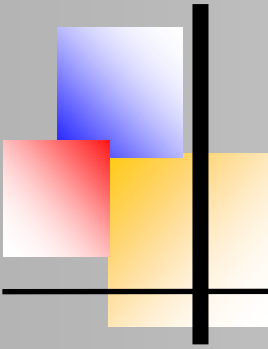
After the publication of this report, there may be more optimal configurations in the sense of feedback.

The observatory

My equipment is housed in the iTelescope facility at Siding Spring Observatory (SSO), NSW Australia (Fig.1). It is one of Australia's most outstanding sites for optical observations, with institutions from around the world converging with their own observatories on the edge of an extinct volcano. iTelescope operates an observatory at SSO housing about 25 telescopes where I rent an observation station. The observatory has a retractable roof, which is controlled by the iTelescope weather station and whose opening and closing is controlled externally.



Fig. 1: The iTelescope facility, Siding Spring Observatory, NSW Australia



My set-up

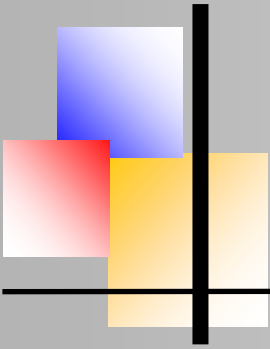
My permanently assigned observation station (Fig. 2) consists of a Paramount MX mount and a PC housed in a cabinet, with the telescope mount being controlled with the program "The SkyX". The main scope is a Planewave CDK 12.5 with a built-in focuser. I record the spectra with the UVEX made by Shelyak Instruments and the recently released motor unit using the Alpy Guiding Unit and the Alpy Calibration Unit.

Spectra are recorded with an Atik 460EX science camera guided by a ZWO ASI174MM guide camera. In order to be able to access NIR and IR, a ZWO EFW with a wavelength filter $< 5300 \text{ \AA}$ is used. In addition, there is a photometric setup on the main telescope using a Takahashi Sky 90 with a ZWO EFW with BVRI filters and a ZWO ASI183M imaging camera. Focus is adjusted using Robofocus.

SSO is managed by the Australian National University. One of the benefits of operating from this site is that the broadband connection is super fast by Australian standards. So I control my observation station from my home in Sydney with the "Teamviewer" program.



Fig. 2: The iTelescope facility, Siding Spring Observatory, NSW Australia



Justification for the automation

While I enjoy observing in real time, I no longer have the stamina to stay up late to acquire spectra. Also, since I pay rent for my observation site and observatory, I want to maximize observing time, which prompted the search for a set-and-forget system.

My skill base

Since I installed my equipment at SSO in 2015, I have been dealing with astrophotography using 'ACP Observatory Control' software quite successfully until 2020. I am not an engineer, programmer or scientist; during the day I work in the field of corporate law. The last course I took in programming was to operate the Radio Shack TRS-80 personal computer in 1980. Aside from videos of the excellent sessions on using Python for Spectroscopy provided by Shelyak in 2021, I am completely self-taught. As a result, I had to use standard software for my system.

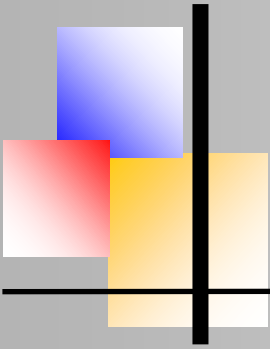
Other alternatives

I know of some observers using Prism. This is a single program to control all elements of the system. The 2SPOT team use it very successfully in Chile. I experimented with it and concluded it wasn't right for me. The scripting system seems straightforward but for what I wanted to do it is particularly involved. There were some challenges with platesolving my small FOV and syncing my Paramount with Prism. I am sure that I could have overcome these with the assistance of other users on the Prism forum but I decided to explore other alternatives.

I understand that ACP has also been used successfully for spectroscopy but it required more customization than I was comfortable with. Similarly approaches using Ineos and Python were beyond my skill base.

The challenge

To me, the biggest challenge for automation is to get the target on the slit of my spectroscope. This requires much greater precision than is called for in astrophotography. In my case, with x2 binning in my guidescope, the slit is only 4 pixels wide – my plate scale is 0.88 arcseconds per pixel. However, the greatest impediment is software design – imaging programs are designed for AP. They assume that the imaging/science camera not only takes images, it is used to focus the telescope and to platesolve images; the guider simply guides. For us, the science camera takes spectra only. We use the guide scope for focusing, plate solving and guiding. The solution I found was to use „Voyager Array“.



BAV MAGAZINE SPECTROSCOPY



Automating spectroscope observations

Voyager

Voyager is similar to other automation programs in that it manages other astro software rather than replacing them. Where it differs is that it can work with a wider set of software packages. For example, for imaging, it will work with Maxim DL, The SkyX, any ASCOM camera and the drivers specific to particular camera such as ZWO. Guiding can be done with Maxim DL, TSX or PHD2.

Out of the (metaphorical) box, it can manage the mount, imaging, guiding, plate solving, autofocusing, take weather data, sky quality data and safety data and control certain web switches which are used for managing observatories. It is also able to run external programs and scripts.

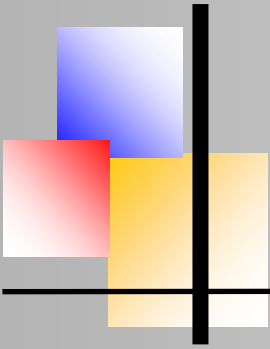
Observation sessions are managed by DragScripts. A series of actions is built up by a user by dragging the requisite task from a list of actions. The series is then saved as a new file and run when necessary. There is considerable flexibility in these actions so that the tasks can be run in the right sequence at the right time. Most helpfully for novices like me, this doesn't require any knowledge of coding – it's a simple click and drag exercise.

Voyager Advanced has recently been released. This enables the user to select a series of targets with certain constraints and leave it to Voyager to determine what to image and when. For now, this can't be applied to spectroscopy – though I hope its added soon.

Voyager Array

Voyager Array was designed to provide users to operate several imaging rigs at once. It assumes that the equipment sits on a single mount and that there are multiple scopes or other imaging devices. There is a dedicated instance of Voyager for each imager which can be run on a single or multiple PCs. The master instances manages slewing, plate solving, guiding and responding to weather and other safety events. The other instances (slaves or nodes) can autofocus, manage their filter wheels and rotators and take images but nothing more. This is the critical feature of my set up.

Maxim DL allows the same camera to be installed as both the imaging camera and guiding camera if the camera is connected as an ASCOM camera. Provided Maxim doesn't send instructions to take images in both instances at the same time, there is no conflict. In my set up, I have my ASI174M set as both imaging and guide camera in Maxim. This is the imaging set up for the master instance of Voyager. I then have a second instance set with my spectroscope camera as the imaging camera.



Stripped back to the essentials, here is the sequence of key tasks:

Slew to designated RA and Dec – master.

Autofocus – master -using guide camera as imaging camera. Calibrate guider – master – using guide camera as guider. Precision slew – master – using guide camera as imaging camera. Commence guiding – master – using guide camera as guider. Take spectra – slave

The precision slew is important. This is similar to the Closed Loop Slew feature in TSX. Voyager will slew to a target, take an image and plate solve it. If allowed by the mount control software, it will sync the mount to that location. It will then slew again and repeat the process. As Paramounts do not allow external syncing, Voyager simply determines the pointing error, makes a corrective slew and repeats the process. Voyager will do this up to 5 times. Importantly, the user sets the acceptable tolerance for this precision slew. I have it set presently to 0.8 arcseconds.

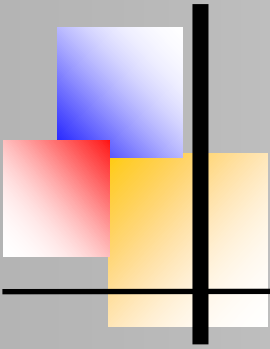
Offset calculation

Of course, a spectroscope slit is rarely in the centre of an image. To use the above approach, we need to determine the RA and Dec for an image to get the target on the slit. Manually, a user can slew and ‘jog’ the mount till the target is on the slit. Then take an image of the field and plate solve it – the centre RA and Dec becomes the target for Voyager.

After much tinkering, I have written a couple of simple Python programs that does the work for me. I input the target name or co-ordinates, provide a link to a plate solved image and provide the x and y pixels for the centre of the image and my preferred slit position. The program then tells me the required RA and Dec to position that target on the slit. My mount is a GEM so the determined offset is only valid for one side of the meridian so I break up my imaging into east and west sequences.

An alternative approach to pointing

My method relies on accurate plate solving of guider images to place the target on the slit. Voyager does not select the target, it simply slews to the designated RA and Dec. Another approach is to use software to automatically select the target from a preset region of interest and use guider pulses to shift that target onto the slit. Some observers use the ‘Restore Lock’ function in PHD2 to do this manually and I believe that Prism also facilitates this. There may be ways of integrating this approach in Voyager although it is not available in the current release of the software.



BAV MAGAZINE SPECTROSCOPY



Automating spectroscope observations

I have written simple Python scripts to turn the flat and ArNe lamp in the Alpy calibration unit on and off. So a standard imaging run for a target and reference star will be as follows:

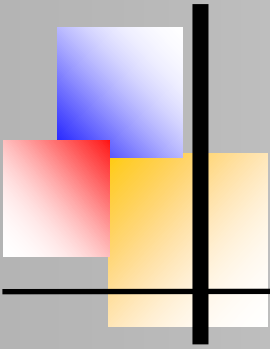
1. Wait till an hour before commencement of imaging
2. Link Array instances
3. Connect Array software ie connect to all equipment, turn on camera coolers.
4. Wait till nautical night
5. Home the mount -master
6. Slew to preselected field – usually 0 Dec and 1 hour in RA before or after meridian
7. Autofocus – using master only ie the telescope using the guider.
8. Calibrate guider
9. Take flat frames – slave – turn on flat lamp, take flats and turn off flat lamp.
10. Wait for astronomical night
11. Precision slew to reference star – master
12. Take ArNe frames – slave – turn on lamp, take frames and turn off lamp
13. Start guider and take reference star spectra – master and slave
14. Precision slew to target star – master
15. Take ArNe frames – as above
16. Start guider and take target star spectra – as above
17. Park telescope and disconnect equipment.

I take a single line text file from the iTelescope weather station which reports the roof status. It is updated every 15 seconds. If the roof closes, Voyager stops the sequence, turns tracking off and waits for the roof to reopen. It then restarts the system, returns to the sequence that was interrupted and starts again.

Once this is all set, its relatively easy to add a third instance to run the photometry set up. I can autofocus the telescope and photometry set up independently and can take spectra and photometry data at the same time. I've also recently started to adjust the grating angle to access different wavelengths. Voyager manages the EFW to set the blocking filter if I am imaging in the NIR or IR.

Constraints

It is important to note that this method is not suitable for all observers. Here are a few things that are required to use this approach:



BAV MAGAZINE SPECTROSCOPY



Automating spectroscope observations

1. Permanent set up – while I am sure there are users who are able to set up in the field quickly and efficiently, it will be hard to achieve the necessary precision in slewing without a permanent set up.
2. Weather – as with any automated system, users need to have some system to manage inclement weather – or have great confidence in the accuracy of your local weather report.
3. Precision slewing – its critical that your set up can achieve the necessary precision to get the target on the slit reliably. With my rig, Voyager can bring an initial pointing error of 1.5arcminutes down to less than an arcsecond with 4 – 5 slews. You need to take advantage of any mount tweaks available to you – I use a 200 point TPoint model, PEC and Protrack.
4. FOV – your guider field of view needs to be wide enough to reliably plate solve. The ASI174 provides a nice and wide field. I have a field of 15 x 9 arcminutes to work with though off-axis aberrations makes it smaller in practice. I use the ATLAS catalog down to mag 19 for Pinpoint or the Gaia catalog in TSX for plate solving. It can be a challenge when imaging away from the Milky Way sometimes but my plate solves rarely fail.
5. Patience – as with anything in this game, you need plenty of this. I never seem to have enough.

Resources

You can find out more about Voyager here: <https://software.starkeeper.it>

The wiki for Voyager is quite helpful. You can access it here: <https://wiki.starkeeper.it>

I posted about using Array on the Voyager forum here: <https://forum.starkeeper.it/t/spectroscopy-witharray/>

My coding is pretty ugly – but if you would like a copy of my offset calculation Python scripts, just drop me an email – peter@oblaw.net.au